The Canadian Journal of Mineralogy and Petrology
ISSN 2817-1713
Vol. 61, pp. 609-622 (2023)
DOI: 10.3749/2200062

ALKALI SULFATES WITH APHTHITALITE-LIKE STRUCTURES FROM FUMAROLES OF THE TOLBACHIK VOLCANO, KAMCHATKA, RUSSIA. IV. APHTHITALITE–PALMIERITE REGULAR INTERGROWTHS: CRYSTALLOGRAPHY, CHEMISTRY, AND GENESIS

NADEZHDA V. SHCHIPALKINA[§], NATALIA N. KOSHLYAKOVA, AND IGOR V. PEKOV

Faculty of Geology, Moscow State University, Leninskie Gory, 119991 Moscow, Russia

ATALI A. AGAKHANOV

Fersman Mineralogical Museum of the Russian Academy of Sciences, Leninsky Prospekt 18-2, Moscow, 119071 Russia

SERGEY N. BRITVIN

Department of Crystallography, St Petersburg State University, University Embankment 7/9, 199034 St Petersburg, Russia

MARIA A. NAZAROVA

Institute of Volcanology and Seismology, Far Eastern Branch of Russian Academy of Sciences, Piip Boulevard 9, 683006 Petropavlovsk-Kamchatsky, Russia

ABSTRACT

The first discovery of regular intergrowths of aphthitalite $K_3Na(SO_4)_2$ and palmierite $K_2Pb(SO_4)_2$ are reported. Crystals of aphthitalite, intergrown with lamellae of palmierite (up to 15 μm thick), along with grains of arcanite, occur in encrustations recovered from the active Arsenatnaya fumarole (Tolbachik volcano, Kamchatka, Russia). These were studied using a combination of scanning electron microscopy, electron probe microanalysis, powder X-ray diffraction, and electron backscatter diffraction techniques. Three types of grain boundaries involving intergrowths of aphthitalite and palmierite were observed: (1) those with a misorientation angle of 60° relative to [001] (twinning), (2) those parallel to the (001) plane, and (3) those with a misorientation angle of 60° relative to [001]. The twinned aphthitalite domains are related by a two-fold rotation about [001] (Dauphiné twin law). The heating of aphthitalite crystals containing palmierite lamellae at 400, 600, and 750 °C shows a nearly complete redistribution and gradual dissolution of palmierite in the aphthitalite matrix. The character of solid-state transformations in the K_2SO_4–Na_2SO_4–$PbSO_4$ system during cooling is controlled by the structural similarity of aphthitalite-type sulfates and palmierite, which contain topologically identical $^2[M(SO_4)_2]$ (M = Na, Pb) layers.

Keywords: aphthitalite, palmierite, metathénardite, alkali sulfate, twinning, oriented intergrowth, EBSD, fumarole sublimate, Tolbachik volcano.

INTRODUCTION

Aphthitalite, ideally $K_3Na(SO_4)_2$, and palmierite, $K_2Pb(SO_4)_2$, are members of a large family of oxysalts having densely packed crystal structures. This family includes more than one hundred sulfates, phosphates, arsenates, molybdates, vanadates, and tungstates (Moore 1973, 1981, Nikolova & Kostov-Kytin 2013, Natarajan *et al*. 2019, and references therein). Most of these compounds are considered potentially useful industrial materials having interesting luminescent, ion-conducting, ferroelastic, or scintillating features (Solodovnikov *et al*. 2017 and references therein).

[§] *Corresponding author e-mail address*: estel58@yandex.ru

Both aphthitalite (previously referred to as *glaserite*) and palmierite were described as new minerals in fumarolic exhalations of the famous Vesuvius volcano, Campania, Italy (Smithson 1813, Lacroix 1907). Aphthitalite and other alkali sulfates having the aphthitalite-type crystal structure, including metathénardite (Na_2SO_4), belomarinaite ($KNaSO_4$), and natroaphthitalite [$KNa_3(SO_4)_2$], all of which are common in exhalation encrustations in the active fumaroles of the Tolbachik volcano, Kamchatka, Russia (Filatov *et al*. 2019, Pekov *et al*. 2020, Shchipalkina *et al*. 2020a, 2021, and references therein). In the last two decades, aphthitalite-group sulfates have also been reported from fumaroles of Vesuvius (Balassone *et al*. 2019 and references therein) and some other volcanoes, *e.g*., Oldoinyo Lengai in Tanzania (Genge *et al*. 2001), Etna in Italy, Krafla and Fimmvorduhals in Iceland (Balić-Žunić *et al*. 2016), *etc*. Metathénardite, belomarinaite, and natroaphthitalite are only known to occur in volcanic fumaroles, whereas aphthitalite is a more geologically widespread mineral, being found in oceanic and lacustrine evaporates and occasionally being found in concentrations that are high enough to make it an important "ore" component in some potassium salt deposits (Eugster 1980, Spencer 2000). Palmierite is a rare mineral, only known from volcanic fumaroles. Several finds of palmierite with this origin were described at Vesuvius (Zambonini 1921, Bellanca 1946, Von Saalfeld 1973); later this mineral was reported from the Merapi volcano in Indonesia (Symonds 1993) and Tolbachik (Pekov *et al*. 2020). Experiments involving the placement of silica tubes into fumarolic vents (having a gas-flow temperature of 760 °C) of the Satsuma-Iwojima volcano show the appearance of the assemblage of aphthitalite, thénardite, and palmierite on the outer walls (Africano *et al*. 2002). Palmierite also forms in anthropogene counterparts of volcanic fumaroles (sublimate assemblages in lead-rich metallurgical slags, *e.g*., Blejesti, Romania; Hansen *et al*. 2019).

The presence of Pb (up to 501 ppm) in aphthitalite from fumaroles at the Piton de la Fournaise volcano, Reunion Island, has been reported (Vlastelic *et al*. 2013). Experiments in silica tubes placed in hot vents in the crater of the Colima volcano, Mexico, show that the aphthitalite-like sulfates that develop are enriched in Zn, Cu, V, and Pb. However, quantitative chemical data needed to further explore the incorporation of these elements is lacking (Taran *et al*. 2000).

In the present paper, the discovery of oriented intergrowths of aphthitalite-palmierite is reported, along with a discussion of the crystal-chemical and genetic aspects of solid-state transformations in the K_2SO_4–Na_2SO_4–$PbSO_4$ system.

Background Information

The general formula for aphthitalite-type compounds is: ${}^{X}X_{(0,1)}{}^{XII}Y_{(0,3)}[{}^{VI}M(TO_4)_2]$, where X and Y = Na, K, Rb, Cs, Ca, Sr, Ba, Ag, Tl, Pb; M = Na, Mg, Ca, Sc, Y, *Ln*, Ti, Zr, Hf, V, Cr, Mo, Mn, Fe, Co, Ni, Cu, Zn, Cd, Al, In, Tl, Ge, Sn, Sb; and T = S, Si, P, Se, V, Cr, Mo, W, Re, Fe, Ru (Lazoryak 1996, Nikolova & Kostov-Kytin 2013). Palmierite-type compounds have the general formula ${}^{X}Y_2[{}^{VI}M(TO_4)_2]$ and, while considered distinct from aphthitalite-type compounds (Moore 1973, Nikolova & Kostov-Kytin 2013), both possess the same principal structural unit: a ${}^{2}[M(TO_4)_2]$ layer, consisting of corner-sharing MO_6 octahedra and TO_4 tetrahedra (Nikolova & Kostov-Kytin 2013) and having fully occupied M and T sites. However, the arrangements of the TO_4 tetrahedra in the ${}^{2}[M(TO_4)_2]$ layer differ between palmierite- and aphthitalite-type structures (Fig. 1). The charge of this layer is important, as it regulates the composition of the X and Y sites. In aphthitalite-type compounds, two types of cation sites are located between the ${}^{2}[M(TO_4)_2]$ layers: X (point symmetry $\bar{3}2/m$) and Y (point symmetry $3m$), these being coordinated by 12 and 10 oxygen atoms, respectively. In aphthitalite [$K_3Na(SO_4)_2$, space group $P\bar{3}m1$] the X site is mainly occupied by K, the Y site by disordered K and Na with K predominating, and the M site by Na. The crystal structure of palmierite (space group $R\bar{3}m$) was first determined by Bellanca (1946) using material from Vesuvius and later refined by Von Saalfeld (1973). In this crystal structure, Pb is coordinated by six O atoms at the M site and K is coordinated in a 10-fold polyhedron (Y site with point symmetry $3m$). Following the topological-geometrical approach suggested by Moore (1973, 1981), the main difference between aphthitalite- and palmierite-type structures relates to the arrangement of interlayer cations and stacking sequence of polyhedral walls (Fig. 2) along the **c** axis. The c parameter in the palmierite unit cell is tripled in comparison with aphthitalite, while the a values of both are similar.

Occurrence

Aphthitalite-group minerals are major components at the studied site, along with minerals of the langbeinite–calciolangbeinite series (Pekov *et al*. 2022), among the alkali-bearing sulfates in deposits of active fumaroles of the Tolbachik volcano. Being easily water-soluble, they are not preserved in extinct fumaroles exposed to atmospheric water. However, encrustations of aphthitalite-group minerals in still hot fumaroles of the Great Tolbachik Fissure Eruption, 1975–1976 (GTFE) and the Tolbachik Fissure Erup-

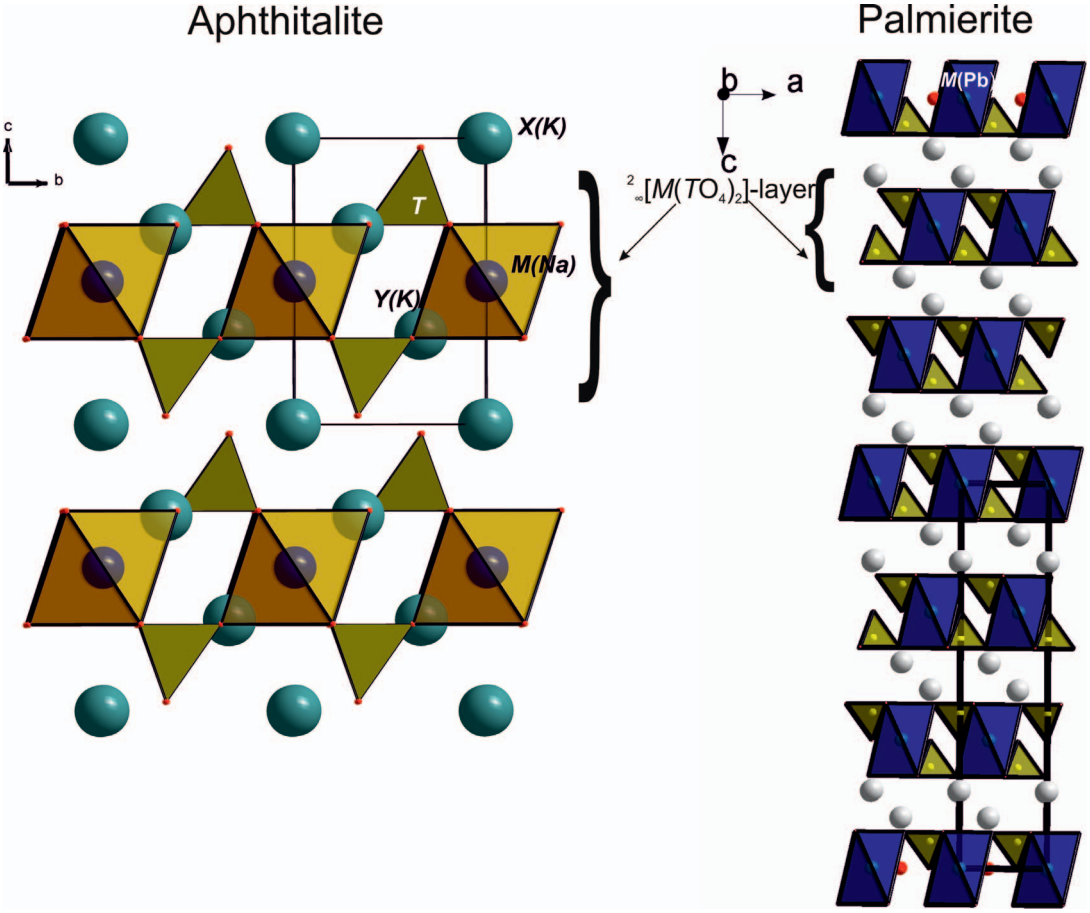

FIG. 1. The crystal structures of aphthitalite (drawn after Okada & Ossaka 1980) and palmierite (drawn after Tissot *et al*. 2001). The unit cells are outlined, along with the MO_6 and YO_{10} polyhedra.

tion, 2012–2013, can still be observed. Note that in papers devoted to Tolbachik fumaroles that were published prior the middle of 2010s, all these minerals were mentioned under the collective name "aphthitalite". The detailed mineralogical and crystal-chemical studies performed in the last decade showed that the Tolbachik "aphthitalite" is in fact a complicated family of related minerals, with significant chemical, structural and, thus, species diversity. Besides aphthitalite, this family includes the above-mentioned new aphthitalite-group minerals, metathénardite, belomarinaite, and natroaphthitalite, along with the related species bubnovaite and dobrovolskyite. These minerals were described in detail in several papers (Gorelova *et al*. 2016, Filatov *et al*. 2019, Pekov *et al*. 2019, Shchipalkina *et al*. 2020a, 2021, Shablinskii *et al*. 2021). Here only two key points are to be made: (1) the richest occurrences of aphthitalite-like minerals at Tolbachik belong to the Main fumarole field of the Second scoria cone of the Northern Breakthrough of the GTFE and (2) as previous studies have shown, aphthitalite in the Tolbachik fumaroles is a relatively rare mineral and significantly less widespread compared to metathénardite or belomarinaite. Aphthitalite is found mainly among products related to the breakdown of high-temperature hexagonal, metathénardite-type solid solutions (Shchipalkina *et al*. 2021).

Palmierite is a common mineral in two active fumaroles, Yadovitaya and Arsenatnaya, in the same Main fumarole field of the Second scoria cone. In encrustations of the Yadovitaya fumarole, it is the major Pb-bearing mineral and is associated with hematite, piypite, alumoklyuchevskite, steklite, sanidine (including its As-bearing variety), lammerite, mcbirneyite, starovaite, lyonsite, pseudolyonsite, averievite, cupro-

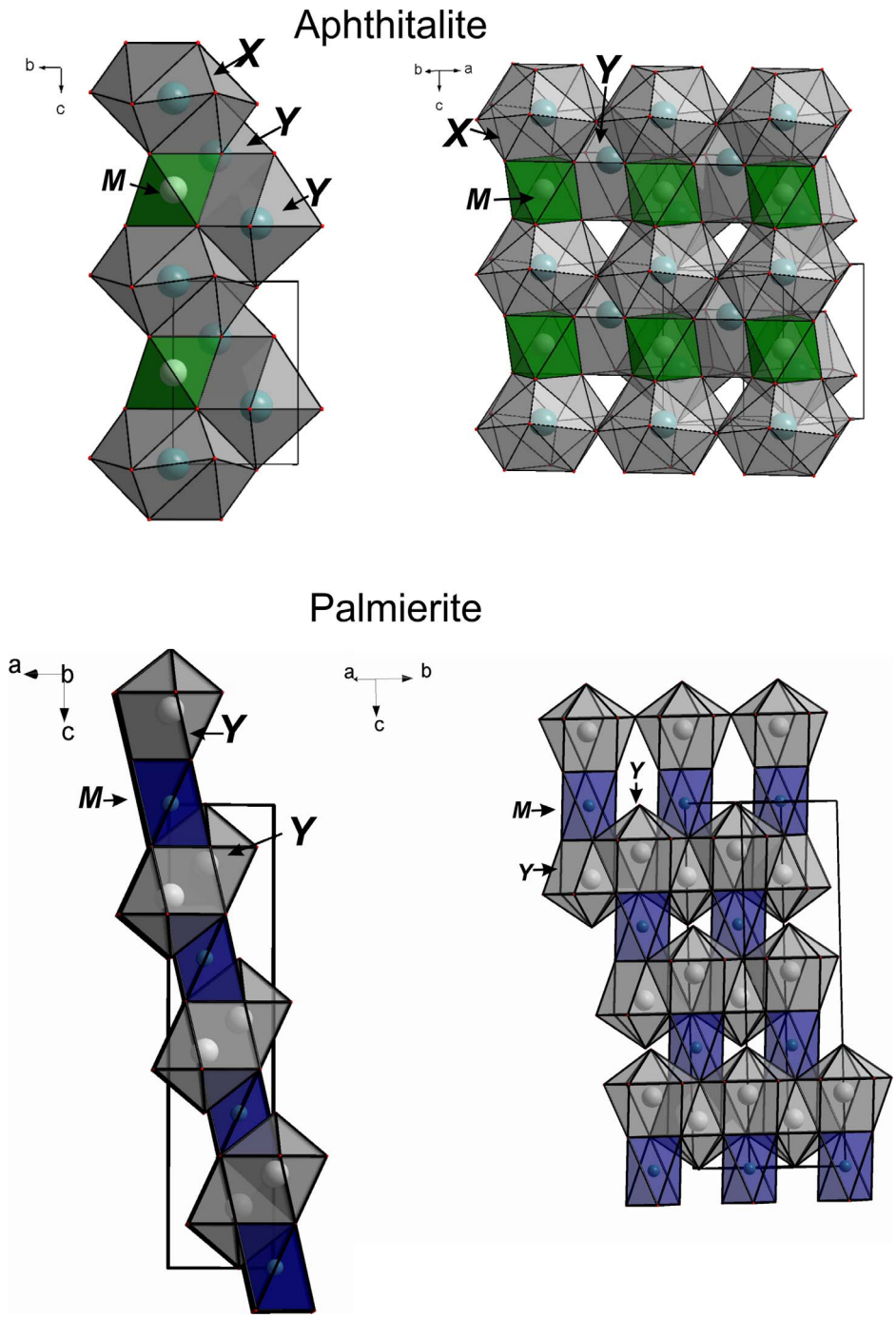

FIG. 2. Cationic polyhedral walls in the crystal structures of aphthitalite (drawn after Okada & Ossaka 1980) and palmierite (drawn after Tissot *et al*. 2001), with outlined unit cells. The SO_4 tetrahedra have been removed for clarity.

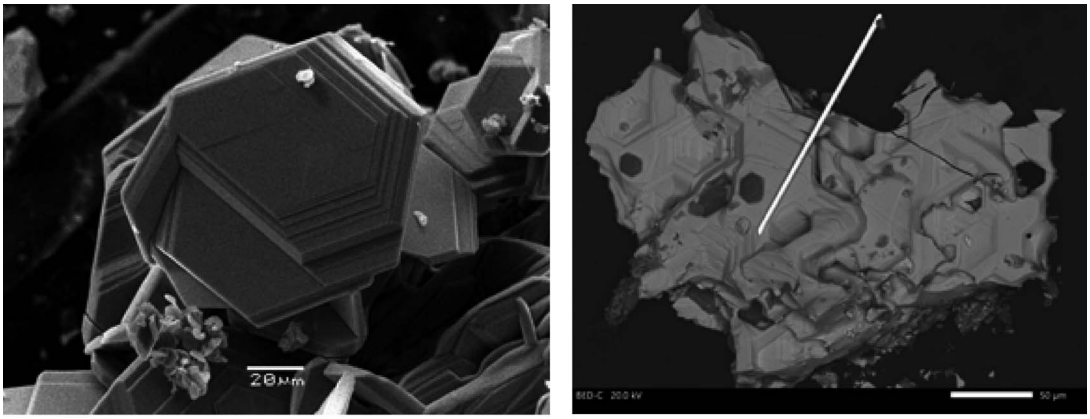

FIG. 3. Palmierite from fumarolic exhalations of the Tolbachik volcano: (a) a cluster of crystals from the Yadovitaya fumarole; (b) a parallel intergrowth (crust) of crude crystals, overgrown by small, hexagonal, tabular crystals of belomarinaite (dark gray; crystals of both sulfates are in parallel orientation) and an elongated crystal of native gold (white needle) from the Arsenatnaya fumarole. SEM images, (a) SE and (b) BSE modes.

molybdite, corundum, and minerals of the langbeinite–calciolangbeinite, lammerite-β–borisenkoite, bradaczekite–zincobradaczekite, and rutile–tripuhyite series. At the Arsenatnaya fumarole, palmierite is the major host to Pb in the middle, polymineralic zone (for description of the zonation of Arsenatnaya, see Shchipalkina *et al.* 2020b). In the upper sulfate-rich zone, the main Pb-bearing mineral is anglesite. At the Arsenatnaya fumarole, palmierite is closely associated with different arsenates (including lammerite, lammerite-β, ericlaxmanite, johillerite, nickenichite, bradaczekite, urusovite, alarsite, pharmazincite, *etc.*), hematite, tenorite, Cu-rich gahnite, fluoborite, native gold, anhydrite, and krasheninnikovite. Other sulfates include those of the aphthitalite group and langbeinite–calciolangbeinite series; these overgrow palmierite and are thus paragenetically later than it. In both fumaroles, palmierite usually forms hexagonal or trigonal lamellar or tabular crystals, up to 0.2 mm (rarely up to 1 mm) across. They range from being euhedral to anhedral, commonly with hexagonal, triangular, or rhomb-like growth figures on the pinacoid {001} face. The lateral faces are represented by the hexagonal prism {100} and unindexed rhombohedra. The crystals are combined in open-work clusters or parallel to near-parallel intergrowths to form crusts (Fig. 3). Palmierite is transparent or semitransparent, colorless, with strong vitreous luster. In some samples, an epitaxial overgrowth of aphthitalite-group minerals on palmierite was observed (Fig. 3b). Chemically, crystals of palmierite from both fumaroles are usually close to endmember $K_2Pb(SO_4)_2$ (#1 in Table 1), with some specimens from Arsenatnaya being Ca-bearing, the Ca most likely substituting for Pb (#2 in Table 1). Data from single-crystal X-ray diffraction measurements gave the following parameters of hexagonal unit cell for Ca-free palmierite from Arsenatnaya: $a = 5.50(2)$, $c = 20.56(6)$ Å, $V = 539(1)$ Å^3.

EXPERIMENTAL

Electron microscopy and microprobe analysis (EPMA)

Secondary electron images were obtained with a JEOL JSM IT-500 scanning electron microscope operated with an accelerating voltage of 20 kV. The chemical composition of samples (Table 1) was determined using a JEOL JXA-8230 electron microprobe instrument using both WDS and EDS modes at the Laboratory of Analytical Techniques of High Spatial Resolution, Department of Petrology, Moscow State University. The operating conditions included an accelerating voltage of 20 kV and beam current of 20 nA; the beam was rastered on an area 2 × 2 μm. The following standards were used for quantitative analysis: halite (Na), potassic feldspar (K), FeS_2 (S), anorthite (Ca), $Rb_2Nb_4O_{11}$ (Rb), and PbTe (Pb). Contents of other elements with atomic numbers higher than carbon are below detection limits.

Powder X-ray diffraction (PXRD) data

Powder X-ray diffraction data (Fig. 4) were collected using a Rigaku R-AXIS Rapid II diffractometer and an image plate. It used Co$K\alpha$ radiation, was operated at 40 kV and 15 mA, employed a rotating

TABLE 1. CHEMICAL COMPOSITION OF THE STUDIED SULFATES

Constituent	1	2	3	4	5	6	7	8	9	10	10	11	12	13	14	15
								wt.%								
Na_2O	-	-	0.42	-	0.40	1.44	12.14	10.49	10.49	10.38	10.02	9.63	11.54	9.50	10.14	9.51
K_2O	19.55	20.37	21.37	18.43	20.86	46.35	39.46	34.82	33.74	34.16	33.31	33.47	32.72	35.99	37.04	36.72
Rb_2O	-	-	-	-	-	0.31	0.21	0.24	0.19	0.26	0.18	0.17	0.15	0.22	0.23	-
CaO	-	1.68	3.39	3.57	3.63	3.88	-	1.56	1.50	1.63	1.53	1.62	1.43	1.80	1.71	2.53
PbO	46.40	42.92	36.92	40.18	36.81	-	-	4.94	5.10	4.63	7.81	7.73	4.86	5.26	2.27	2.76
SO_3	33.83	35.72	37.76	36.99	37.36	49.34	49.81	47.52	48.49	48.24	47.66	47.07	48.96	48.24	49.42	49.17
Total			99.86	99.16	99.06	101.33	101.61	99.57	99.51	99.30	100.51	99.69	99.66	101.01	100.81	100.69
								formula calculated on whole number of O atoms								
Na	-	-	0.06	-	0.06	0.08	1.26	1.15	1.13	1.12	1.08	1.05	1.22	1.02	1.07	1.01
K	1.97	1.95	1.94	1.72	1.91	1.62	2.70	2.49	2.39	2.43	2.36	2.39	2.27	2.53	2.57	2.55
Rb	-	-	-	-	-	0.01	0.01	0.01	0.01	0.01	0.01	0.01	0.01	0.01	0.01	-
Ca	-	0.13	0.26	0.28	0.28	0.11	-	0.09	0.09	0.10	0.09	0.10	0.08	0.11	0.10	0.15
Pb^{2+}	0.99	0.87	0.70	0.78	0.70	0.00	0.00	0.07	0.08	0.07	0.11	0.11	0.07	0.07	0.03	0.04
S^{6+}	2.01	2.01	2.01	2.03	2.01	1.01	2.01	2.00	2.01	2.00	1.98	1.98	2.00	1.99	2.01	2.01
O	8	8	8	8	8	4	8	8	8	8	8	8	8	8	8	8

1–2 – separate crystals of palmierite (1 – Yadovitaya fumarole, 2 – Arsenatnaya fumarole); 3–7 – aphthitalite with palmierite and arcanite intergrowths (see Fig. 6a) from the Arsenatnaya fumarole: palmierite (3–5), arcanite (6), and aphthitalite matrix (7); 8–15 – bulk composition of the crystals after heat treatment at 400 °C (8–10), 600 °C (10–13), and 750 °C (14–15).

- = Constituent content is below the detection limit.

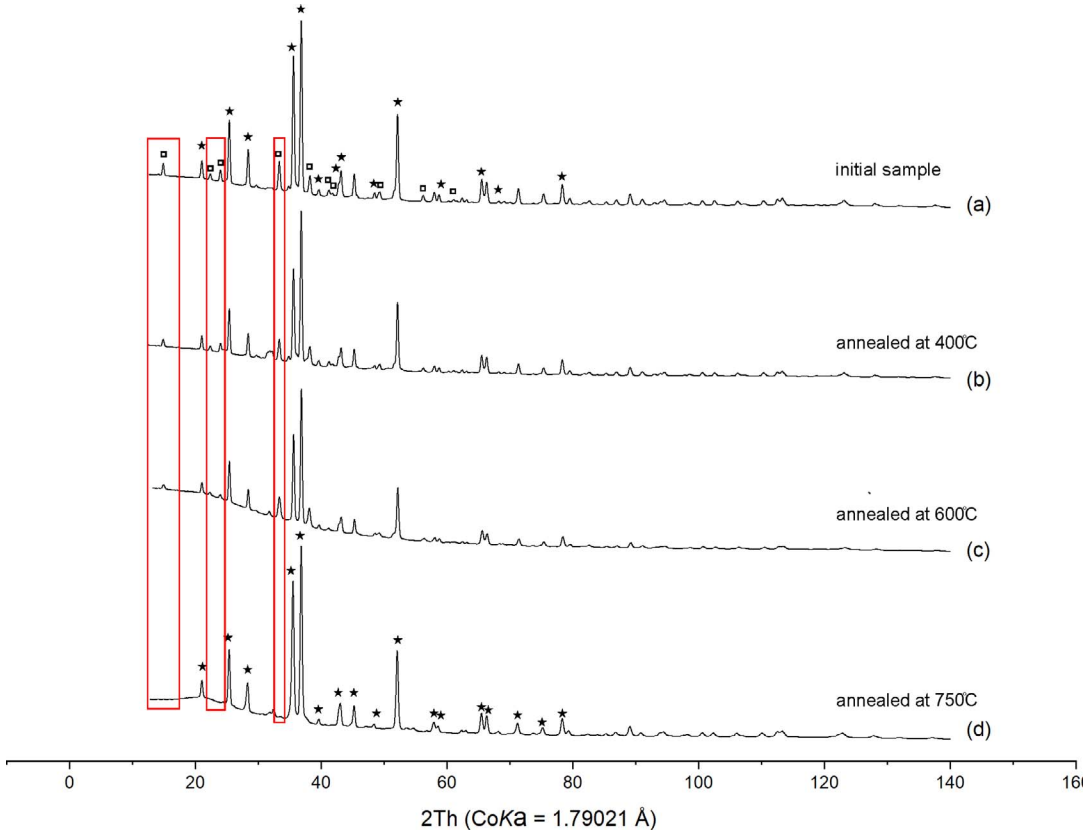

FIG. 4. X-ray powder diffraction patterns of the examined sulfates: (a) the initial sample from the Arsenatnaya fumarole and samples annealed at (b) 400 °C, (c) 600 °C, and (d) 750 °C (see also Figs. 5 and 6). The main diagnostic reflections of aphthitalite are marked as * and palmierite as □.

anode with the microfocus optics, and used Debye-Scherrer geometry ($d = 127.4$ mm) and exposures of 15 min. The data were processed using the osc2xrd program (Britvin *et al*. 2017) and Stoe WinXPOW software.

Electron backscattered diffraction (EBSD)

The orientation of crystals, including sub-individuals in intergrowths, in the samples examined was determined using the EBSD technique on a JEOL JSM IT-500 scanning electron microscope equipped with an Oxford Instruments NordlysMax^2 EBSD system. Data were collected using an accelerating voltage of 30 kV, a working distance of 20 mm, and a stage tilted at 70° (Laboratory of Analytical Techniques of High Spatial Resolution, Department of Petrology, Moscow State University). The system was calibrated using a crystal of synthetic Si; the sample was polished and carbon coated. The EBSD data was collected using Oxford Instruments AZtec HKL software and processed using HKL Channel5 software. Diffraction patterns were collected with a step size of 1.15 μm over a rectangular region of about 150 × 150 μm^2.

SAMPLE DESCRIPTION

Samples containing aphthitalite with palmierite intergrowths were collected from a hot (~300 °C) fumarolic chamber in the intermediate (polymineralic) zone of the Arsenatnaya fumarole (Shchipalkina *et al*. 2020b). Aphthitalite occurs as translucent, whitish single crystals up to 0.35 mm across. The major forms that were observed include the pinacoid {001}, hexagonal prism {100} and rhombohedron {102}. All crystal faces exhibit elements of skeletal growth, including holes and grooves (Figs. 5a, b). Palmierite lamellae (typically up to 2 μm, rarely up to 15 μm thick) are homogeneously distributed throughout the volume of aphthitalite crystals (Figs. 5a and 6a).

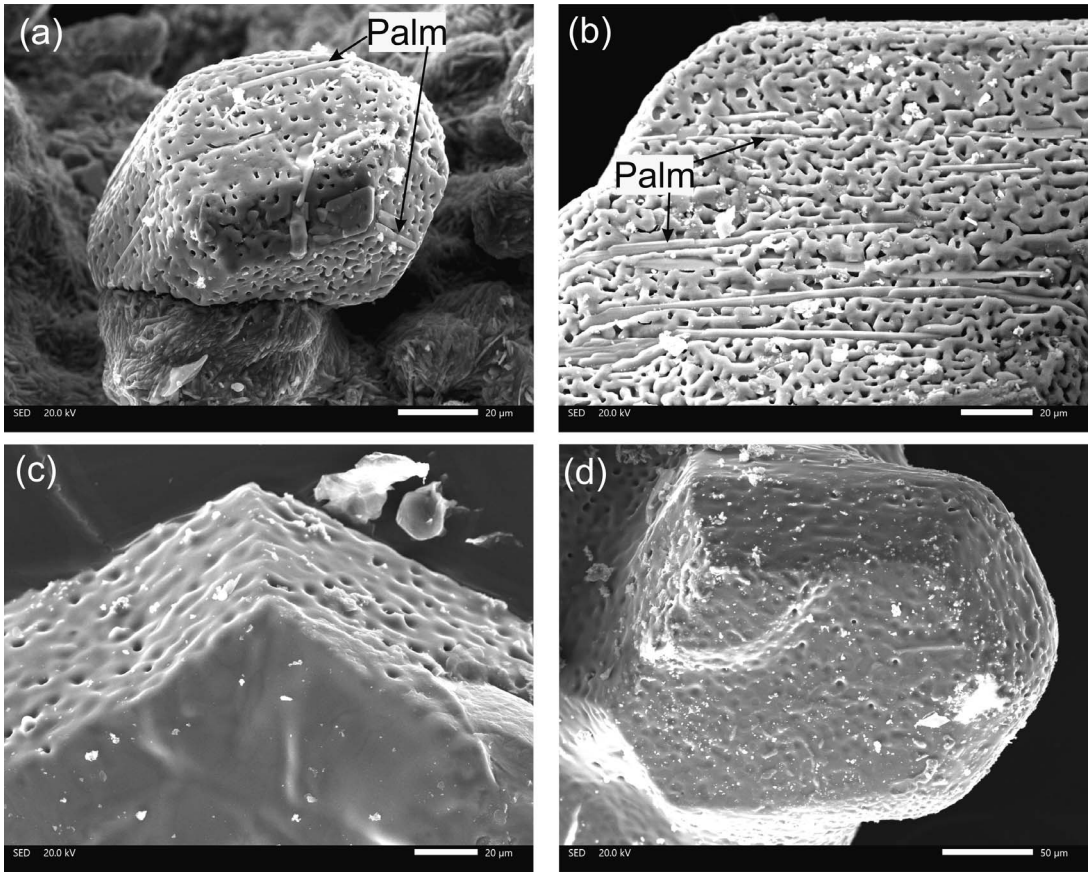

FIG. 5. Images of the crystal surfaces of examined sulfates: (a) the initial sample from the Arsenatnaya fumarole: aphthitalite intergrown with lamellae of palmierite (Palm); (b) the surface of the sample after annealing at 400 °C: aphthitalite with intergrown lamellae of palmierite; (c) and (d) samples after annealing at 600 °C and 750 °C, respectively. Neither shows any palmierite lamellae exposed on the surface. SEM images, SE mode.

RESULTS OF HEATING EXPERIMENTS

After annealing of samples at 400, 600, and 750 °C, the crystals kept their color, semi-transparency, and morphology, with no signs of melting being observed (Fig. 5). It was noted, however, that the surfaces of crystal faces distinctly changed after heating up to 600 and 750 °C, becoming smoother after these experiments and with the palmierite intergrowths disappearing (Figs. 5 and 6). Observations made on polished sections demonstrate that as the annealing temperature increases, the grain boundaries of palmierite lamellae in the aphthitalite matrix become more diffuse and their orientation gradually becomes less distinct, ultimately disappearing (Fig. 6).

The PXRD data are in agreement with the scanning electron microscopy (SEM) results: reflections attributable to palmierite are observed in all PXRD patterns except for that for that annealed at 750 °C, wherein only aphthitalite reflections are observed. The intensities of palmierite reflections gradually decrease as temperature increases (Fig. 4). At temperatures <600 °C, the unit-cell parameters of aphthitalite in the samples examined are constant: $a = 5.67$, $c = 7.30$ Å, $V = 203$ Å^3. The homogeneous phase that is observed at 750 °C has the following unit-cell parameters: $a = 5.668(2)$, $c = 7.322(3)$ Å, $V = 204.6(1)$ Å^3.

DISCUSSION

The regularly arranged lamellae of palmierite in aphthitalite crystals before heat treatment are parallel (or near-parallel) to the pinacoid {001} face (Fig. 5), suggesting a crystallographic relationship between the two. The EBSD map, given in Euler coloring (ϕ_1 blue, Φ red, ϕ_2 green), shows there are two main

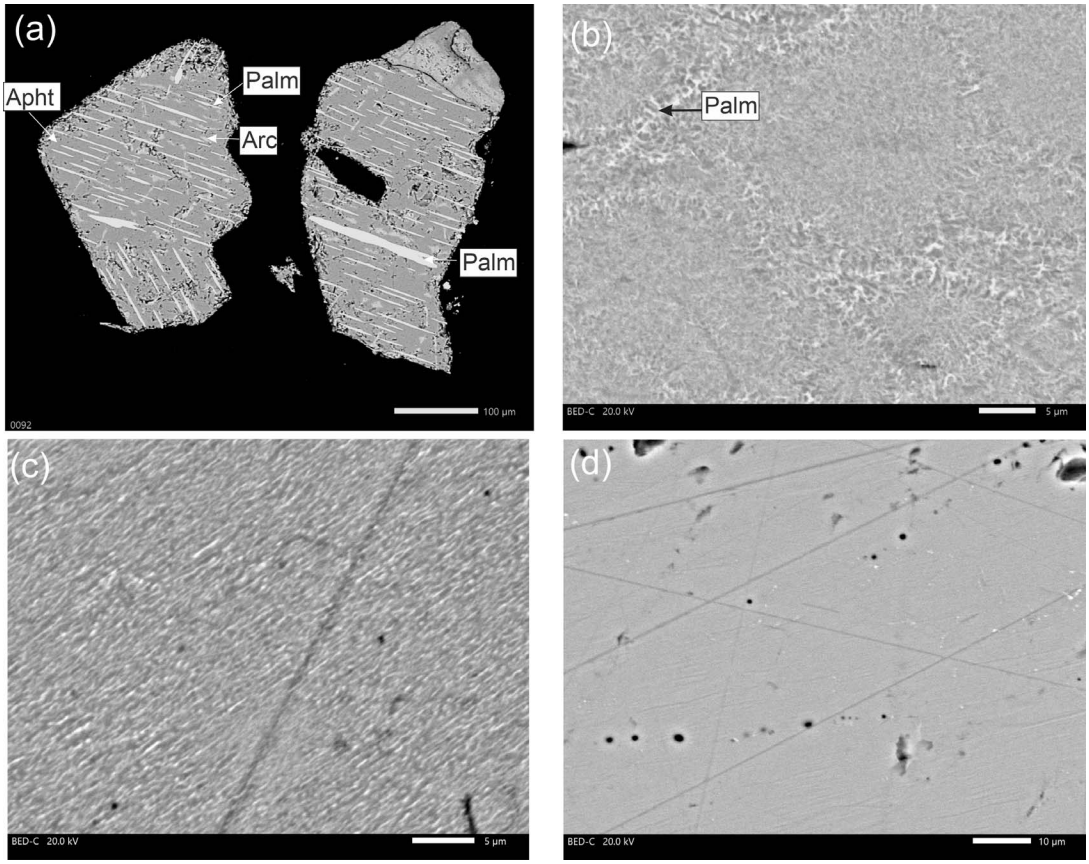

FIG. 6. Images (polished sections) showing (a) the initial sample with palmierite (Palm) and arcanite (Arc) intergrowths in aphthitalite (Apht) and samples annealed at (b) 400 °C, (c) 600 °C, and (d) 750 °C. SEM images, BSE mode. See also Figure 5.

orientations involving intergrown aphthitalite and palmierite, these being shown in blue and violet Euler colors in Figure 7. For simplicity, areas showing admixed langbeinite with individuals of aphthitalite and palmierite having other orientations are omitted (painted light gray) (Fig. 7). Domains of both aphthitalite and palmierite are aligned along the **c** axis, being offset by 60°, as shown in the pole figures and unit-cell schemes (Fig. 8). The aphthitalite domains are presumably twin domains related *via* a two-fold axis parallel to the three-fold **c** axis (*i.e.*, being expressed by the matrix [$\bar{1}00$; $0\bar{1}0$; 001]) (Fig. 9). This leads to a rotation of 60 or 180°, an element of 6/*mmm* holohedry. This twin law (merohedral twinning) is well-known in trigonal crystal structures and also occurs in rhombohedral crystals (obverse-reverse twinning) (Herbst-Irmer & Sheldrick 2002, Hahn & Klapper 2013). The twin individuals of aphthitalite occupy areas up to 2500 μm^2 within the crystal and have irregular borders. The palmierite lamellae are not twinned and are located inside or cross the edges of differently oriented large aphthitalite blocks. Thus, the orientation of palmierite crystals may coincide with the orientation of the aphthitalite matrix or may be related to it by the same "twin law." Thus, there are three types of boundaries in the studied crystals: (1) aphthitalite-aphthitalite intergrowths being related by a misorientation angle of 60° about [001] (twin boundary), (2) aphthitalite-palmierite intergrowths having similar orientations, and (3) aphthitalite-palmierite intergrowths being related by a misorientation angle of 60° in relation to [001].

The observed aphthitalite-palmierite intergrowths can arise through solid-state transformation during cooling. The above-discussed twin law is based on the symmetry operation of the 6/*mmm* holohedry that describes the crystal structure of high-temperature solid solution of the K_2SO_4–Na_2SO_4 system (space

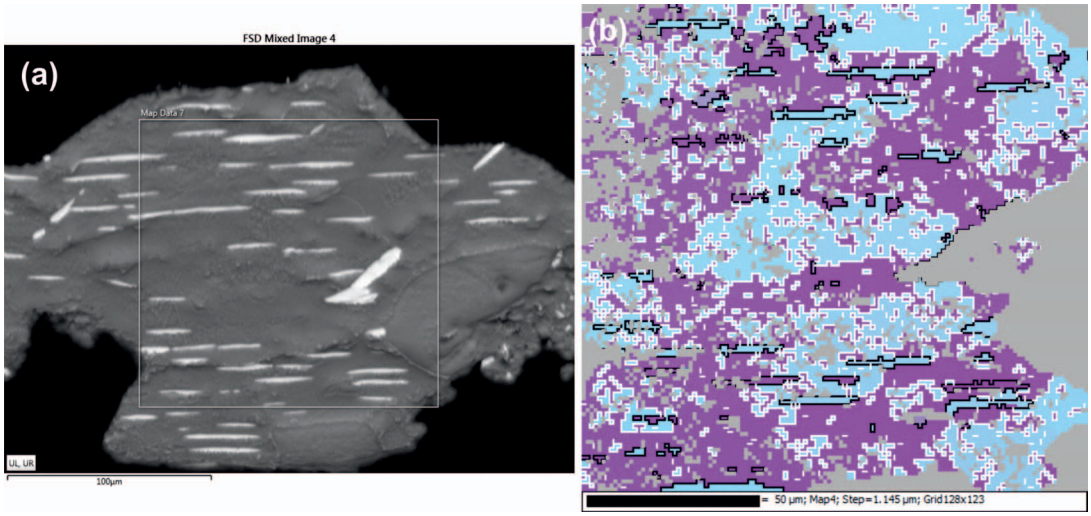

FIG. 7. The oriented intergrowths of aphthitalite-palmierite from the Arsenatnaya fumarole before heating. (a) BSE image, (b) orientation EBSD map of the surface in Euler coloring (ϕ_1 blue, Φ red, ϕ_2 green). White lines show borders between aphthitalite crystals with misorientation angle between [100] direction 60 ± 5°; black lines correspond to aphthitalite-palmierite phase boundaries.

group $P6_3/mmc$) (Eysel *et al*. 1985, Naruse *et al*. 1987, Pekov *et al*. 2019). This hexagonal (Na,K)-disordered sulfate is considered to have been the parent phase of the aphthitalite-group minerals found in the Tolbachik fumaroles (Shchipalkina *et al*. 2021). Its transition to trigonal sulfates having aphthitalite-like structures (aphthitalite, natroaphthitalite, or belomarinaite, depending on the Na:K ratio) can be explained by ordering of K and Na, which induces transformation twinning. Note, the same type of suppression involving a six-fold axis (namely the two-fold rotation) occurs during the well-known $\alpha \rightarrow \beta$ phase transition in quartz and, as a result, the twins related to the two-fold rotation along [001] appear, giving rise to so-called Dauphiné twins. Twinning in aphthitalite and related sulfates, including belomarinaite and natroaphthitalite, is also a known phenomenon. As shown by Yu *et al*. (1988), there are several twin laws characteristic of the synthetic double sulfate $KNaSO_4$, including: (1) a twin axis parallel to the *c* axis, (2) twin axes parallel to the two-fold [110] axes, and (3) having (110) as the twin plane. Both belomarinaite and natroaphthitalite, which were recently described from Tolbachik fumaroles, are also susceptible to twinning. Refinement of their crystal structures the presence of twinning expressed by the twin matrix $[\bar{1}00; 0\bar{1}0; 001]$, which corresponds to twinning by a two-fold rotation along [001] (Shchipalkina *et al*. 2020a).

Aphthitalite twin domains in the crystals studied in the present work are irregular in shape, whereas the palmierite domains have planar boundaries and form lamellar intergrowths with equal widths of domains (Fig. 7).

For palmierite, a ferroelastic transformation can be proposed (Hahn & Klapper 2013, and references therein). The palmierite-aphthitalite boundaries are considered to be parallel to the (001) plane. The stacking of aphthitalite and palmierite domains in the samples that were examined may be explained by the alternation of the aphthitalite- and palmierite-type $^2[M(TO_4)_2]$ layers (Fig. 1). The aphthitalite-palmierite intergrowths are characterized by the stacking lamellae up to 2 µm thick (equal to approximately three thousand unit cells), which collectively give rise to platy crystals (Fig. 5). Note also the parallel, epitaxial overgrowth of belomarinaite on palmierite in other specimens from the Arsenatnaya fumarole (Fig. 3b).

Besides palmierite, in some crystals of aphthitalite the K_2SO_4 phase occurs as intergrowths that are irregular in shape (Fig. 6a). Both the arrangement and morphology of these intergrowths suggest they represent an orthorhombic modification of K_2SO_4, *i.e*., arcanite, rather than the high-temperature hexagonal polymorph α-K_2SO_4, which is structurally related to the aphthitalite. It is considered thus that lamellae of α-K_2SO_4 could adopt the same (parallel) orientation in an aphthitalite matrix, as seen with palmierite

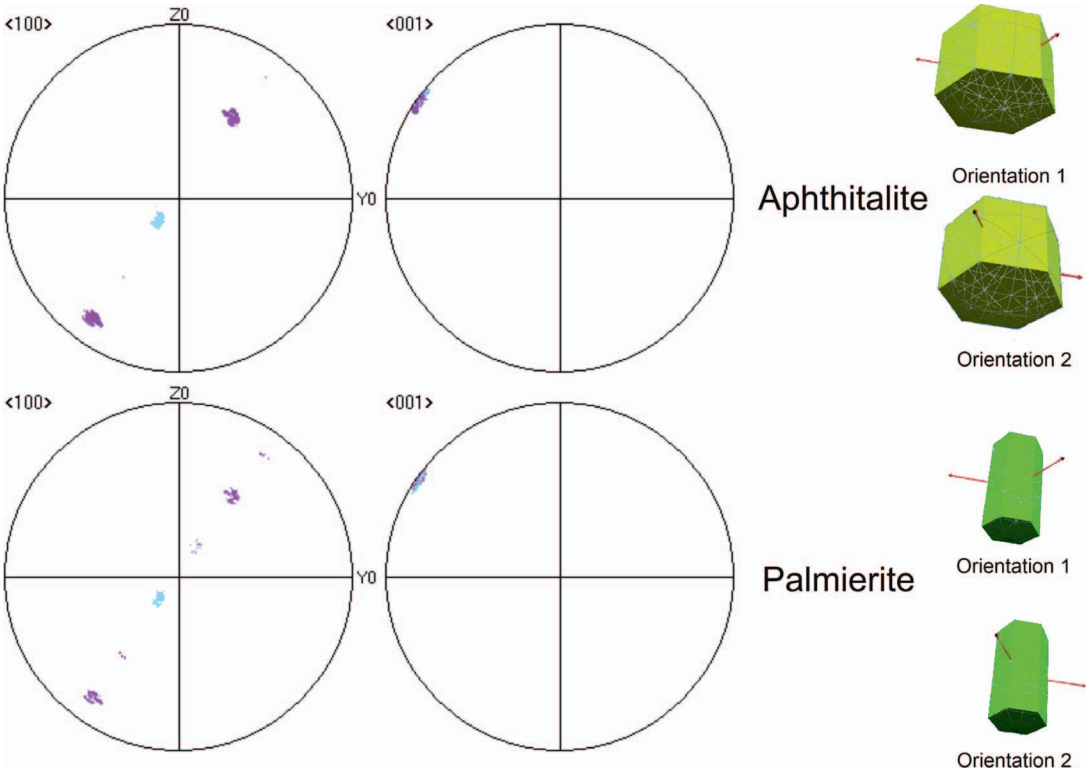

FIG. 8. The {100} and {001} pole figures showing the relationships between the domains of aphthitalite and palmierite. Blue and violet areas on pole figures correspond to the orientation of <100> and <001> of aphthitalite and palmierite domains given in Euler coloring as on the EBSD orientation map (Fig. 7). The misorientation angle between aphthitalite and palmierite domains is 60°. The difference between the two orientations is shown by the models of crystals with the outlined axis.

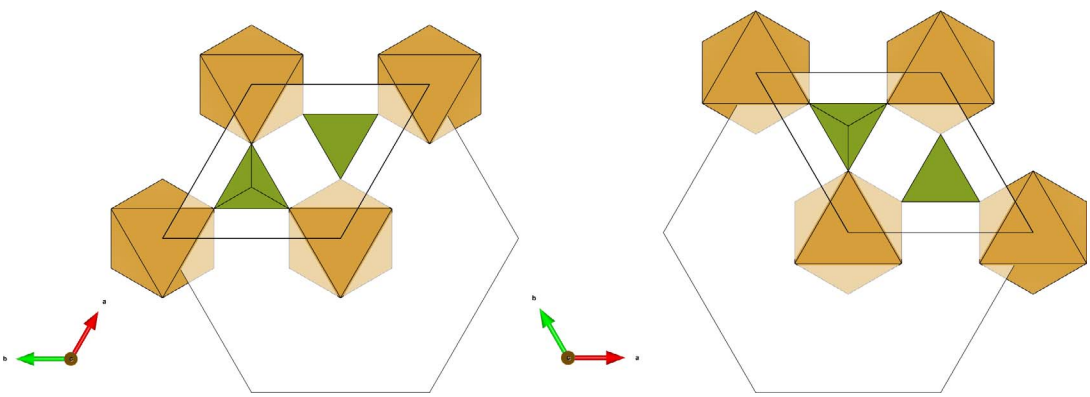

FIG. 9. Projections of the aphthitalite crystal structure along [001] for two twin individuals, related by rotation with the two-fold axis parallel to the three-fold axis. Cations at the *X* site are removed. The Na-centered octahedra (*Y*) are yellow-brown and the SO_4 tetrahedra are green.

lamellae, owing to the topological similarity between them.

As annealing experiments demonstrate, heating leads to the gradual redistribution of palmierite in the aphthitalite matrix. The size of the palmierite domains decrease until their complete dissolution in aphthitalite has occurred. This indirectly suggests the possible incorporation of Pb into the crystal structure of the initial high-temperature sulfate. The same mechanism was earlier reported for impurities of K, Ca, Zn, Cu, and Mg in impurity-rich varieties of metathénardite from the Tolbachik fumaroles, these being given the general, simplified formula $(Na,K,Zn,Cu,Mg)_{2-x}SO_4$ (Pekov *et al*. 2019). Such impurities could, on one hand, help to stabilize the metathénardite structure and, on the other hand, they could initiate the solid-state transformation in high-temperature alkali sulfates having aphthitalite-like crystal structures, as well as contributing to the development of exsolution-type features (Shchipalkina *et al*. 2021). The most widespread type of exsolution is associated with the Na-rich part of the K_2SO_4–Na_2SO_4 system. Aphthitalite is the K-richest known sulfate having the aphthitalite-type structure, so it is thought that the initial phase may have been even richer in K than aphthitalite. The excess of K in a primary high-temperature solid solution with a metathénardite-type crystal structure could lead to the segregation of arcanite and aphthitalite during cooling, as suggested by the phase diagram for the K_2SO_4–Na_2SO_4 system (Eysel *et al*. 1985), results from the current study, and those given in Shchipalkina *et al*. (2021) and references therein. Thus, aphthitalite, arcanite, and palmierite are suggested to be the products of the solid-state transformation of a primary, metathénardite-like, high-temperature phase with the assumed simplified formula $(K,Na,Pb)_{2-x}(SO_4)$. The incorporation of Pb in a K-rich, high-temperature parent phase may have contributed to the segregation of palmierite, which has a crystal structure topologically similar to that of aphthitalite. Thus, the preference of solid-state transformations in the K_2SO_4–Na_2SO_4–$PbSO_4$ system encountered during cooling is considered to have been controlled by crystal-chemical factors.

Conclusions

Encrustations from an active, oxidizing-type fumarole, Arsenatnaya, at the Tolbachik volcano (Kamchatka, Russia), were found to contain regular aphthitalite-palmierite intergrowths. These were examined using a combination of SEM, EPMA, PXRD, and EBSD techniques, supported by heat-treatment experiments, data which were used to demonstrate that these intergrowths formed by the solid-state transformation of an initial, high-temperature, hexagonal, K-rich and Pb-bearing sulfate phase during cooling. This phase had an aphthitalite-like (probably metathénardite-type) crystal structure and the assumed formula $(K,Na,Pb)_{2-x}(SO_4)$. The arrangement of aphthitalite and palmierite domains is crystallographically controlled, owing to the similarity of their close-packed crystal structures. For aphthitalite, it was determined that the transformation twinning is consistent with a Dauphiné twin law (two-fold rotation about [001]), and for palmierite, a ferroelastic transformation is hypothesized. The stacking of aphthitalite and palmierite domains parallel to the (001) plane is explained as being an alternation of the aphthitalite- and palmierite-type $^2[M(SO_4)_2]$ (M = Na and Pb, respectively) layers, which are topologically the same in the crystal structures of both minerals.

Acknowledgments

The authors thank Travis Olds and an anonymous reviewer for valuable comments and Henrik Friis and Andrew McDonald for editorial work. The work of NVS, NNK, and IVP (mineralogical studies, heating experiments, SEM, EPMA, and EBSD) is supported by the Russian Science Foundation, grant no. 19-17-00050. The technical support by the SPbSU X-Ray Diffraction Resource Center is acknowledged.

References

Africano, F., Van Rompaey, G., Bernard, A., & Le Guern, F. (2002) Deposition of trace elements from high temperature gases of Satsuma-Iwojima volcano. *Earth Planets Space* **54**, 275–286.

Balassone, G., Petti, C., Mondillo, N., Panikorovskii, T.L., de Gennaro, R., Cappelletti, P., Altomare, A., Corriero, N., Cangiano, M., & D'Orazio, L. (2019) Copper minerals at Vesuvius Volcano (Southern Italy): A mineralogical review. *Minerals* **9**, 730.

Balić-Žunić, T., Garavelli, A., Jakobsson, S.P., Jonasson, K., Katerinopolous, A., & Acquafredda, P. (2016) Fumarolic Minerals: An Overview of Active European Volcanoes. *In* Updates in Volcanology – From Volcano Modeling to Volcano Geology (K. Nemeth, ed.). IntechOpen, London, United Kingdom.

Bellanca, A. (1946) La struttura della palmierite. *Periodico di Mineralogia*, **15**, 5–25 (in Italian).

Britvin, S.N., Dolivo-Dobrovolsky, D.V., & Krzhizhanovskaya, M.G. (2017) Software for processing the X-ray powder diffraction data obtained from the curved image plate detector of Rigaku RAXIS Rapid II diffractometer. *Zapiski Rossiiskogo Mineralogicheskogo Obshchestva* **146**(3), 104–107 (in Russian).

Eugster, H.P. (1980) Geochemistry of evaporitic lacustrine deposits. *Annual Reviews of Earth Planet Science* **8**, 35–63.

Eysel, W., Hoefer, H.H., Keester, K.L., & Hahn, T. (1985) Crystal chemistry and structure of Na_2SO_4 (I) and its solid solutions. *Acta Crystallographica* **B41**, 5–11.

Filatov, S.K., Shablinskii, A.P., Vergasova, L.P., Saprikina, O.Y., Bubnova, R.S., Moskaleva, S.V., & Belousov, A.B. (2019) Belomarinaite $KNa(SO_4)$: A new sulphate from 2012–2013 Tolbachik Fissure Eruption, Kamchatka Peninsula, Russia. *Mineralogical Magazine* **83**, 569–575.

Genge, M.J., Balme, M., & Jones, A.P. (2001) Salt-bearing fumarole deposits in the summit crater of Oldoinyo Lengai, Northern Tanzania: Interactions between natrocarbonatite lava and meteoric water. *Journal of Volcanology and Geothermal Research* 106, 111–122.

Gorelova, L.A., Vergasova, L.P., Krivovichev, S.V., Avdontseva, E.Yu., Moskaleva, S.V., Karpov, G.A., & Filatov, S.K. (2016) Bubnovaite, $K_2Na_8Ca(SO_4)_6$, a new mineral species with modular structure from the Tolbachik volcano, Kamchatka peninsula, Russia. *European Journal of Mineralogy* 28, 677–686.

Hahn, T. & Klapper, H. (2013) Twinning of crystals. *In* International Tables for Crystallography. Wiley, Hoboken, New Jersey, United States of America (413–483).

Hansen, S., Montero-Ruiz, I., Rovira, S., Steiniger, D., & Toderas, M. (2019) The earliest lead ore processing in Europe. 5th millennium BC finds from Pietrele on the Lower Danube. *PLoS ONE* **14**(4), e0214218.

Herbst-Irmer, R. & Sheldrick, G.M. (2002) Refinement of obverse/reverse twins. *Acta Crystallographica Section B* **B58**, 477–481.

Lacroix, A. (1907) Les minéraux des fumerolles de l'éruption du Vésuve en avril 1906. *Bulletin de la Société Française de Minéralogie* 30, 219–266.

Lazoryak, B.I. (1996) Design of inorganic compounds with tetrahedral anions. *Russian Chemical Reviews* **65**(4), 287–305.

Moore, P.B. (1973) Bracelets and pinwheels: A topological-geometrical approach to the calcium orthosilicate and alkali sulfate structures. *American Mineralogist* **58**, 32–42.

Moore, P.B. (1981) Complex crystal structures related to glaserite, $K_3Na[SO_4]_2$: Evidence for very dense packings among oxysalts. *Bulletin of Mineralogy* **104**(4), 536–547.

Naruse, H., Tanaka, K., Morikawa, H., Marumo, F., & Mehrotra, B.N. (1987) Structure of Na_2SO_4 at 693 K. *Acta Crystallographica* **B43**, 143–146.

Natarajan, S., Surendran, D., Vadivel, G., & Krishnasamy, S. (2019) Impact of cerium doping on dielectric properties of palmierite $K_2Pb(SO_4)_2$. *Journal of Electronic Materials* **48**, 2577–2586.

Nikolova, R. & Kostov-Kytin, V. (2013) Crystal chemistry of «glaserite» type compounds. *Bulgarian Chemical Communications* **45**(4), 418–426.

Okada, K. & Ossaka, J. (1980) Structures of potassium sodium sulphate and tripotassium sodium disulphate. *Acta Crystallographica* **B36**, 919–921.

Pekov, I.V., Shchipalkina, N.V., Zubkova, N.V., Gurzhiy, V.V., Agakhanov, A.A., Belakovskiy, D.I., Chukanov, N.V., Lykova, I.S., Vigasina, M.F., Koshlyakova, N.N., Sidorov, E.G., & Giester, G. (2019) Alkali sulfates with aphthitalite-like structures from fumaroles of the Tolbachik volcano, Kamchatka, Russia. I. Metathénardite, a natural high-temperature modification of Na_2SO_4. *The Canadian Mineralogist* **57**(6), 885–901.

Pekov, I.V., Zubkova, N.V., Agakhanov, A.A., Chukanov, N.V., Belakovskiy, D.I., Sidorov, E.G., Britvin, S.N., Turchkova, A.G., & Pushcharovsky, D.Y. (2020) Eleomelanite, $(K_2Pb)Cu_4O_2(SO_4)_4$, a new mineral species from the Tolbachik Volcano, Kamchatka, Russia. *The Canadian Mineralogist* **58**(5), 625–636.

Pekov, I.V., Zubkova, N.V., Galuskina, I.O., Kusz, J., Koshlyakova, N.N., Galuskin, E.V., Belakovskiy, D.I., Bulakh, M.O., Vigasina, M.F., Chukanov, N.V., Britvin, S.N., Sidorov, E.G., Vapnik, Y., & Pushcharovsky, D.Yu. (2022) Calciolangbeinite-*O*, a natural orthorhombic modification of $K_2Ca_2(SO_4)_3$, and the langbeinite–calciolangbeinite solid-solution system. *Mineralogical Magazine* **86**(4), 557–569.

Shablinskii, A.P., Filatov, S.K., Krivovichev, S.V., Vergasova, L.P., Moskaleva, S.V., Avdontseva, E.Y., Knyazev, A.V., & Bubnova, R.S. (2021) Dobrovolskyite, $Na_4Ca(SO_4)_3$, a new fumarolic sulfate from the Great Tolbachik fissure eruption, Kamchatka Peninsula, Russia. *Mineralogical Magazine* **85**, 233–241.

Shchipalkina, N.V., Pekov, I.V., Chukanov, N.V., Belakovskiy, D., Zubkova, N.V., Koshlyakova, N.N., Britvin, S.N., & Sidorov, E.G. (2020a) Alkali sulfates with aphthitalite-like structures from fumaroles of the Tolbachik volcano, Kamchatka, Russia. II. A new mineral, natroaphthitalite, and new data on belomarinaite. *The Canadian Mineralogist* **58**(2), 167–181.

Shchipalkina, N.V., Pekov, I.V., Koshlyakova, N.N., Britvin, S.N., Zubkova, N.V., Varlamov, D.A., & Sidorov, E.G. (2020b) Unusual silicate mineralization in fumarolic sublimates of the Tolbachik volcano, Kamchatka, Russia – Part 1: Neso-, cyclo-, ino- and phyllosilicates. *European Journal of Mineralogy* **32**, 101–119.

Shchipalkina, N.V., Pekov, I.V., Britvin, S.N., Koshlyakova, N.N., & Sidorov, E.G. (2021) Alkali sulfates with aphthitalite-like structures from fumaroles of the Tolbachik volcano, Kamchatka, Russia. III. Solid solutions and exsolutions. *The Canadian Mineralogist* 59(4), 713–727.

Smithson, J. (1813) On a saline substance from Mount Vesuvius. *Philosophical Transactions of the Royal Society of London* 103, 256–262.

Solodovnikov, S.F., Atuchin, V.V., Solodovnikova, Z.A., Khyzhun, O.Y., Danylenko, M.I., Pishchur, D.P., Plyusnin, P.E., Pugachev, A.M., Gavrilova, T.A., Yelisseyev, A.P., Reshak, A.H., Alahmed, Z.A., & Habubi, N.F. (2017) Synthesis, structural, thermal, and electronic properties of palmierite-related double molybdate α-$Cs_2Pb(MoO_4)_2$. *Inorganic Chemistry* **56**(6), 3276–3286.

Spencer, R.J. (2000) Sulfate Minerals in Evaporate Deposits. *In* Sulfate Minerals: Crystallography, Geochemistry, and Environmental Significance (C.N. Alpers, J.L. Jambor, & D. Nordstrome, eds). *Reviews in Mineralogy & Geochemistry* 40, 173–192.

Symonds, R. (1993) Scanning electron microscope observations of sublimates from Merapi Volcano, Indonesia. *Geochemical Journal* **26**, 337–350.

Taran, Y.A., Bernard, A., Gavilanes, J-C., & Africano, F. (2000) Native gold in mineral precipitates from high-temperature volcanic gases of Colima volcano, Mexico. *Applied Geochemistry* **15**, 337–346.

Tissot, R.G., Rodriguez, M.A., Sipola, D.L., & Voigt, J.A. (2001) X-ray powder diffraction study of synthetic palmierite, $K_2Pb(SO_4)_2$. *Powder Diffraction* **16**(2), 92–97.

Vlastelic, I., Stadacher, T., Deniel, C., Devidal, J.L., Devouard, B., & Finizola, A. (2013) Lead isotopes behavior in the fumarolic environment of the Piton de la Fournaise volcano (Reunion Island). *Geochimica et Cosmochimica Acta* **100**, 297–314.

Von Saalfeld, H. (1973) Crystallographic investigations of Glaserite from Mount Vesuvius (Italy). *Neues Jahrbuch für Mineralogie, Monatshefte* **2**, 75–78.

Yu, J.T., Tsai, S-F., & Chen, R.H. (1988) Detection of twinning in $KNa(SO_4)$ crystals by electron paramagnetic resonance and by X-ray diffraction. *Physical Review B* **38**(16), 147–155.

Zambonini, F. (1921) Sur la palmiérite du Vésuve et les mineraux qui l'accompagnent. *Comptes Rendus Hebdomadaires des Séances de l'Académie des Sciences* **172**, 1419–1422.

Received October 11, 2022. Revised manuscript accepted February 2, 2023.

This manuscript was handled by Associate Editor Henrik Friis and Editor Andrew McDonald.